Neoplasma 2024; 71(1): 48–59

doi:10.4149/neo_2024_231018N544

The role of polyethylenimine-functionalized gold nanoclusters carrying plasmid CMTM5 in impeding the malignant progression of prostate cancer cells by promoting EGFR endocytosis

Linjin LI[1,#], Chengpeng LI[1,#], Feilong MIAO[1], Wu CHEN[1], Xianghui KONG[1], Ruxian YE[1], Rui FENG[2,*]

[1]*Department of Urology, The Third Clinical Institute Affiliated to Wenzhou Medical University, The Third Affiliated Hospital of Shanghai University, Wenzhou People's Hospital, Wenzhou, Zhejiang, China;* [2]*Department of Urology, Zhenjiang Hospital of Chinese Traditional and Western Medicine, Zhenjiang, Jiangsu, China*

**Correspondence: 13913439473@139.com*
[#]Contributed equally to this work.

Received October 18, 2023 / Accepted January 25, 2024

In this research, polyethylenimine-functionalized gold nanoclusters (PEI-AuNCs) were synthesized for the delivery of plasmid CMTM5 (pCMTM5) to prostate cancer (PCa) cells, with the objective of elucidating the mechanism underlying its anticancer efficacy. The PEI-AuNCs loaded with pCMTM5 (PEI-AuNCs@pCMTM5) tumor-targeting drug delivery system was established. Subsequently, both the obtained PEI-AuNCs and PEI-AuNCs@pCMTM5 underwent characterization through a transmission electron microscope (TEM) and dynamic light scattering (DLS). Employing RT-qPCR, western blot, flow cytometry, immunofluorescence, and co-immunoprecipitation (co-IP) assays, the consequences of CMTM5 overexpression on the expression of EGFR were investigated. Moreover, the influence of PEI-AuNCs@pCMTM5 on PC-3 cells was assessed through CCK-8, wound healing assay, and Transwell experiments. As a result, the PEI-AuNCs and PEI-AuNCs@pCMTM5 were presented as uniformly dispersed spherical with stable particle sizes and positive charges, showcasing favorable dispersion within the solution. In comparison to Lip2000, the PEI-AuNCs demonstrated superior transfection efficiency and lower cellular toxicity. Following the overexpression of CMTM5, the proliferative capacity of PC-3 cells was markedly suppressed, while both migratory and invasive abilities exhibited noteworthy reduction, with the efficacy of PEI-AuNCs@pCMTM5 consistently outperforming that of free pCMTM5. Subsequent mechanistic investigations unveiled that CMTM5 does not directly inhibit the synthesis of EGFR or facilitate its degradation, but rather influences the endocytic process of EGFR. In conclusion, the PEI-AuNCs nano-delivery system exhibits good biocompatibility and efficaciously conveys pCMTM5 to PCa cells. Crucially, pCMTM5 does not directly interact with EGFR, and CMTM5 governs the malignant progression of PC3 cells by promoting EGFR endocytosis.

Key words: polyethylenimine-functionalized gold nanoclusters; CMTM5; prostate cancer; EGFR; endocytosis

Prostate cancer (PCa) stands as the second most prevalent malignancy among males worldwide, accompanied by a staggering mortality rate of up to 7.1% [1]. Despite a comparatively lower incidence of PCa in China than in Western countries, factors such as aging demographics, environmental pollution, and a shift towards a Westernized dietary pattern have contributed to a significant upward trend in PCa incidence [2, 3]. Common strategies for managing PCa encompass surgery, radiotherapy, chemotherapy, and hormone therapy [4]. Nevertheless, a considerable number of PCa patients inevitably progress to metastatic castration-resistant prostate cancer (mCRPC) [5]. The aforementioned conventional therapies only marginally extend the survival rate of mCRPC patients by 2–4 months, and the prognosis for these patients remains notably poor, with no effective curative methods identified to date [6, 7]. Consequently, there is an imperative need for extensive research into the mechanisms underlying the onset and progression of PCa, with the goal of identifying more efficacious alternative strategies for the treatment of PCa.

Comprehending the molecular pathways governing malignant tumors in PCa is vital for effective targeted therapy.

Among the numerous regulatory molecules in PCa, the aberrant activation of the epidermal growth factor receptor (EGFR) assumes a pivotal role in propelling the transition from androgen-dependent PCa to CRPC [8]. Within solid tumors, EGFR can bind with EGF and TNF-α, resulting in the autophosphorylation of EGFR tyrosine kinase, subsequently activating downstream pathways, including ERK/MAPK, PI3K/AKT, Ezrin/NF-κB, and upregulating transcription factors such as Snail and Slug, thereby fostering tumor cell proliferation, migration, and survival [9]. In hormone-dependent PCa, the EGFR signaling pathway manifests distinctive regulatory mechanisms. Despite the recent intensive focus on EGFR in extensive PCa targeted drug research, the outcomes have been modest, mainly attributed to the intricacy of the EGFR pathway in PCa. The activation of the EGFR pathway and the induction of PCa cell development represent a multifaceted regulatory process, with the induction of EGFR endocytosis and its subsequent entry into the lysosomal degradation pathway serving as a crucial mechanism to attenuate EGFR signaling [10].

Numerous molecules possess the capacity to accelerate ligand-induced clearance of EGFR from the cell surface or facilitate ligand-induced degradation of EGFR, thereby governing the EGFR transporting. Upon inhibition of the expression regulation of these molecules, persistent activation of EGFR signaling ensues, consequently fostering the progression of cancer [11]. Current research has indicated that CKLF-like MARVEL transmembrane domain-containing family 5 (CMTM5), a recently discovered tumor-suppressive protein involved in the sorting and transport of membrane receptors, may play a role in the transport process of EGFR [12]. CMTM5 exhibits heightened expression in various human normal tissues, yet it is suppressed or absent in multiple malignancies such as liver, lung, and kidney cancer. Elevated expression of CMTM5 significantly diminishes cancer cell proliferation, migration, and invasive capabilities [13]. In PC-3 cells, the reinstatement of CMTM5 expression not only markedly inhibits cell proliferation but also restrains their invasive and migratory capacities [14]. Validation through the PC-3 cell xenograft model has also affirmed that CMTM5 exerts the ability to suppress tumor growth *in vivo* and downregulate the expression of tumor proliferation-related genes [15]. However, while CMTM5 exerts a significantly inhibitory effect on the activation of the EGFR/PI3K/Akt pathway in PCa, it does not directly inhibit EGFR synthesis or facilitate EGFR degradation [16]. Previous reports have indicated that CMTM7 and CMTM8, members of the same family as CMTM5, inhibit signaling pathway activity by inducing EGFR endocytosis, thereby suppressing the progression of cancer [17, 18]. Nonetheless, further exploration is imperative to ascertain whether CMTM5 exerts a comparable regulatory effect in PCa.

Gene therapy emerges as one of the potential approaches for cancer treatment and has been extensively researched. The crux of gene therapy lies in the capacity of gene agents to endure the mildly acidic pH in the tumor microenvironment, selectively deliver to target cells, and do so without manifesting significant toxicity or adverse effects [19]. Additionally, preventing degradation and internalization poses a challenge for gene agents in PCa treatment, which can be addressed through the utilization of nano-delivery systems. An ideal gene delivery system should possess attributes such as biodegradability, non-toxicity, non-immunogenicity, specific targeting, and a reliable capacity to stimulate gene expression [20]. Metal nanoclusters have garnered considerable attention, owing to their extraordinary physical and chemical properties, demonstrating potential applications in optics, catalysts, sensing, targeted imaging, and therapy [21]. Gold nanoclusters (AuNCs), particles with a diameter of less than 2 nanometers, have exhibited immense potential in intracellular delivery and diagnostics, biosensing, bioimaging, drug delivery, and the detection of biomacromolecules (DNA, proteins, enzymes) due to their facile synthesis, high biocompatibility, and robust fluorescent properties [22–25]. The high surface area-to-volume ratio and an affinity for biomacromolecules render AuNCs a judicious selection for gene and drug delivery [26]. Furthermore, functionalizing AuNCs with polymers can further augment their drug-carrying capacity. Polyethylenimine (PEI), a classic cationic agent, possesses the capacity to protect plasmids from degradation and improve lysosomal gene release, thus finding widespread use as a gene transfection vector for both animals and cells [27]. Employing the PEI reduction method enables the acquisition of PEI-functionalized gold nanoclusters (PEI-AuNCs), and the positively charged nature of PEI-AuNCs are more prone to binding with DNA, which carries a negative charge [28]. Through the proton sponge effect, PEI-AuNCs facilitate the delivery of plasmid DNA (pDNA) into cells, subsequently releasing it within the cells, thereby playing a role in protecting and aiding the entry of DNA into the cells, with an efficiency 15 times greater than its counterpart without PEI modification [26].

In this research, AuNCs were synthesized and subjected to subsequent surface modification with PEI. The resulting PEI-AuNCs were employed for the delivery of the tumor-suppressing gene CMTM5 into PC-3 cells. The physicochemical properties and cytotoxicity of PEI-AuNCs were characterized through *in vitro* experiments, subsequently delving into their targeted therapeutic efficacy and elucidating the mechanism of action in delivering CMTM5 for PCa.

Materials and methods

Cell culture. The human cell lines, RWPE-1 and PC-3 cells, were obtained from the American Type Culture Collection (ATCC, Rockville, MD, USA). All cells were maintained in Ham's F-12K medium (Procell) supplemented with 10% fetal bovine serum (FBS, Gibco) at 37 °C in a 5% CO_2 humidified incubator.

Preparation of PEI-AuNCs and PEI-AuNCs@pCMTM5. All glassware used was soaked in freshly prepared aqua regia for 24 h and thoroughly rinsed with ultrapure water before use. In a synthesis flask, 25 µl of 1% $HAuCl_4 \cdot 3H_2O$ solution and 2.5 ml of H_2O were added, and the mixture was stirred for 2 min until homogenized. Subsequently, 1.5 ml of 2.5 mg/ml PEI solution was added, and stirring was continued for 5 min until the solution turned pale yellow. Finally, 80 µl of 0.10 mol/l ascorbic acid was introduced, and stirring continued. After 5 min, the solution turned into a transparent colorless solution, followed by a transition to purple-red within 1 h. The reaction was allowed to proceed for 24 h to yield PEI-AuNCs. Then, 0.5 mg of plasmid CMTM5 (pCMTM5) was added to 10 ml PEI-AuNCs solution. After being magnetically stirred for 24 h, the solution underwent dialysis to eliminate free pCMTM5, ultimately yielding PEI-AuNCs@pCMTM5. Finally, the resultant solution was stored in a refrigerator at 4 °C.

Characterization of PEI-AuNCs and PEI-AuNCs@pCMTM5. Initially, the dispersibility and stability of PEI-AuNCs were assessed in water, PBS, and F12 cell culture medium. The solutions were stored in a cell culture incubator to simulate the cellular growth environment and were preserved for 7 days. Images of the solutions were captured on the 1st, 3rd, and 7th day to observe their states. Additionally, the size and zeta potential of PEI-AuNCs were continuously measured using dynamic light scattering (DLS) for 7 days. For the assessment of the morphological characteristics of the PEI-AuNCs and PEI-AuNCs@pCMTM5, samples were dropped onto a copper grid and subjected to negative staining with a 2% UO_2 acetate aqueous solution. After drying, the morphological changes before and after the encapsulation of pCMTM5 were observed under a transmission electron microscope (TEM; FEI Talos F200S, FEI). The average particle sizes and zeta potential of PEI-AuNCs and PEI-AuNCs@pCMTM5 were measured through DLS.

Cell Counting Kit-8 (CCK-8). RWPE-1 cells and PC-3 cells in 100 µl of complete medium (F-12K containing 10% FBS) were seeded in a 96-well plate at a density of 1×10^4 cells/well and incubated at 37 °C under 5% CO_2 for 24 h. Subsequently, the freeze-dried and collected prepared PEI-AuNCs nanoparticles were subjected to weighing, calculating the corresponding dosage concentration (refers to the concentration of PEI-AuNCs in the cell culture medium). Following this, the freshly prepared PEI-AuNCs suspension at various concentrations of 0, 50, 100, 200, 400, 600, 800, and 1000 µg/ml was introduced into each well containing the seeded cells and further incubated at 37 °C for 24 and 48 h. After determined intervals, 10 µl of CCK-8 solution was added to each well and reacted at 37 °C for 1 h. Cell viability was assessed by measuring the absorbance at 450 nm through a microplate reader. The cell survival rate was calculated as cell viability (%) = [OD450 (sample) – OD450 (blank)]/[OD450 (control) – OD450 (blank)] × 100%.

The transfection efficiency verification. PC-3 cells were cultured on 10 mm^2 glass coverslips placed in 24-well cell culture plates, with a cell density of 5×10^4 cells/well. After a 24 h pre-incubation period, PEI-AuNCs loaded with 2.5 µg pGFP were added. A mixture of commercial transfection reagent Lip2000 with an equivalent amount of pGFP, was used as a control, with the Lip2000 dosage following the usage instructions. After a further 48 h incubation, the cultured cells were washed with PBS and fixed with 4% (V/V) paraformaldehyde. Finally, confocal laser scanning microscopy was employed for cellular imaging to observe and calculate the GFP overexpression efficiency in PC-3 cells.

Electrophoretic mobility shift assay (EMSA). The protective capability of PEI-AuNCs@pCMTM5 complex for pDNA was analyzed by incubating PEI-AuNCs@pCMTM5 with DNase-I. For the analysis, synthesized PEI-AuNPs were centrifuged for 30 min at 12,000×g at 20 °C to obtain the pellet that was then treated with CMTM5 DNA and incubated for 30 min. Subsequently, various concentrations (0.25, 0.5, 1.0, 1.5, and 2.0 µg/µl) of DNase-I were added and incubated for a further period of 30 min. To arrest the activity of DNase-I enzyme, 10% sodium dodecyl sulfide (SDS) was introduced into the solution. The PEI-AuNCs@pCMTM5 was then incubated with heparin sulfate for 30 min. Following the incubation, the samples were electrophoresed on a 1% agarose gel and stained with EtBr for visualization under UV light.

Drug release. Seal 1 ml of free pCMTM5/PEI-AuNCs@pCMTM5 solution in a dialysis bag. Subsequently, place the dialysis bag into 10 ml of PBS and set it on a constant-temperature (37 °C) shaker system. At specific time points (0–72 h), withdraw 1 ml of the dialysate and promptly replenish an equivalent volume of buffer. Utilize a microspectrophotometer (NanoDrop 2000) to measure the concentration of pCMTM5 in the dialysate.

Reverse transcription-quantitative polymerase chain reaction (RT-qPCR). Total RNA was extracted from the cells using the TRIzol reagent, and the RNA's purity was assessed through a UV-visible spectrophotometer. The RNA concentration was then standardized and mixed in a 20 µl reverse transcription reagent. After instantaneous centrifugation, the mixture was placed in a reverse transcription apparatus to convert it into cDNA. Afterward, the mRNA expression levels of CMTM5 and EGFR were quantified using a SYBR Green qRT PCR Master Mix on an ABI 7300 Plus Real-time PCR System, following the manufacturer's instructions. The mRNA expression level was normalized to β-actin expression in the same sample. The relative expression of CMTM5 and EGFR mRNA was calculated using the $2^{-\Delta\Delta Cq}$ method. The PCR primer sequences were shown as follows: CMTM5: 5'-GGAGGACCACATCCGCTAGAT-3' (upstream), 5'-CAGGGAGTGGAAGCAGAT-3' (downstream); EGFR: 5'-GGTCTTGAAGGCTGTCCAACG-3' (upstream), 5'-CCTCAAGAGAGCTTGGTTGGG-3' (downstream); β-actin: 5'-CTGGAACGGTGAAGGTGACA-3' (upstream), 5'-AAGGGACTTCCTGTAACAATGCA-3' (downstream).

Western blot. The total protein was extracted from PC-3 cells using RIPA lysis and extraction buffer, followed by centrifugation at 12,000×g for 10 min at 4 °C, yielding the protein sample in the supernatant. The protein sample concentration was determined using the BCA protein assay kit. The proteins were separated by 10% SDS-PAGE and transferred to a PVDF membrane. After washing with Tris-buffered saline (TBST) at room temperature, the membrane was blocked with skimmed milk in TBS for 1 h. Subsequently, it was incubated with CMTM5 (1:1000; Abcam; ab187980) and EGFR (1: 1000; Abcam; ab52894) antibodies overnight at 4 °C. On the following day, the membrane was washed three times with TBST for 10 min each, followed by incubation with HRP-conjugated IgG secondary antibody at room temperature for 2 h. The membrane was then washed with TBST. The target protein was detected using an ECL chemiluminescence detection kit, with β-actin (1: 5000; Abcam; ab8226) serving as the internal reference. The grey values of the protein bands were calculated using ImageJ software.

Wound healing assay. PC-3 cells were cultured in 6-well plates until they reached 70–80% confluency. Subsequently, the tips of sterile pipette heads were gently used to create straight scratches. The PBS buffer was used to gently wash away the detached cells, and the cells were then cultured in a serum-free co-culture system. Cells from 0 h and 24 h of co-culture were taken separately, and cell migration was observed. Images were captured using an inverted microscope, and the width of the scratch before and after co-culture was measured for analysis using ImageJ software.

Transwell. The Transwell filter chamber underwent pre-coating with Matrigel (50 mg/l) at a ratio of 1:8 at 4 °C for 30 min. PC-3 cells were cultivated in Ham's F-12K medium for 24 h. Subsequently, they were rinsed twice with PBS and resuspended in the medium to achieve a density of 2×10^5 cells/ml. A total of 200 µl of cell suspension/well was introduced into the upper chamber, while 400 µl of medium containing 15% FBS was added to the lower chamber in a 24-well plate. Following an incubation period of 48 h at 37 °C with 5% CO_2, all fixations were carried out using a 4% formaldehyde solution (1 ml) at room temperature for 10 min. After inhaling the stationary fluid, the cells on the upper surface were eliminated using cotton swabs, and those adhering to the bottom of the membrane were stained with 0.1% crystal violet at 37 °C for 30 min. The count of invasive cells was performed under a light microscope (Shanghai Cai Kang Optical Instrument Co., Ltd.) at a magnification ×100 in five randomly selected fields/well.

Analysis of EGFR by flow cytometry. After transfecting PC-3 cells for 48 h, they were subjected to trypsinization and centrifuged at 1500×g for 5 min. The cells were then washed with PBS and fixed with 3% paraformaldehyde at 4 °C for 30 min. Subsequently, they were subjected to blocking and incubation using an anti-EGFR monoclonal antibody (Abcam; ab52894) and fluorescein isothiocyanate (FITC)-conjugated goat anti-rabbit immunoglobulin (Abcam; ab223339). A cell count of 3×10^4 was conducted via flow cytometry (FACSCalibur) with excitation at 488 nm, and the data were analyzed using CELLQuest software (BD Bioscience, USA). This experimental procedure was replicated three times.

Immunofluorescence. Four groups of PC-3 cells subjected to distinct treatments were harvested and fixed with 4% paraformaldehyde, permeabilized in 0.1% Triton-X-100, and blocked with 3% FBS. Subsequently, the cells underwent treatment with the anti-EGFR antibody (Abcam; ab52894) for 1 h, followed by incubation with a FITC-conjugated secondary antibody (Abcam; ab223339) for another hour. This experiment was replicated three times. Cellular imaging was conducted using a Leica TCS SP5 confocal microscope to observe the co-localization of CMTM5 and EGFR within the cells.

Co-immunoprecipitation (co-IP) Assay. The PC-3 cells were rinsed with PBS and subsequently incubated on ice with RIPA lysis buffer for 30 min. After centrifugation for 10 min, the supernatant was collected and incubated with the EGFR antibody or control IgG at 4 °C for 2 h. Subsequently, 20 µl of protein A agarose beads were incubated overnight at 4 °C to facilitate the coupling of the antibody with the protein A agarose beads. Post immunoprecipitation, the mixture was centrifuged at 3,000×g for 3 min at 4 °C, causing the agarose beads to settle at the bottom of the tube. The supernatant was carefully aspirated, and the agarose beads were washed 3–4 times with 1 ml of lysis buffer. Subsequently, 15 µl of 2×SDS loading buffer was added, and the solution was boiled for 5 min. Finally, the western blotting analysis was conducted, identifying the binding proteins through immunoprecipitation, and the target protein was detected using the ECL detection system.

Statistical analysis. The entire dataset was analyzed using SPSS 20.0 and GraphPad Prism 6.0 (GraphPad Software, San Diego, CA, USA). The experimental results are presented as the means ± standard deviation (SD). Student's t-test and one-way analysis of variance were employed to assess differences among groups. A significance level of $p<0.05$ was deemed statistically significant.

Results

Characterization of PEI-AuNCs and PEI-AuNCs@pCMTM5. Evaluation of the dispersion of PEI-AuNCs in water, PBS, and F12 cell culture medium over 1, 3, and 7 days indicated favorable dispersion in all three groups, with no apparent sedimentation observed (Figure 1A). Further assess the average particle size and zeta potential of PEI-AuNCs in the aforementioned three media over a continuous seven-day period, with minimal variations observed (Figures 1B, 1C). Moreover, the average particle size of PEI-AuNCs was examined under different pH conditions (neutral and acidic) over seven days (Supplementary Figure S1A), as well as continuously measured at six time points within the initial

24 h (Supplementary Figure S1B), indicating the stability of PEI-AuNCs. The TEM image reveals that PEI-AuNCs and PEI-AuNCs@pCMTM5 exhibit uniformly dispersed spherical structures (Figure 1D). Additionally, DLS analysis revealed minimal changes in the average particle size and zeta potential before and after the encapsulation of pCMTM5, and the zeta potential result indicated a positive charge on the surface of the composite, affirming the successful modification by PEI (Figures 1E, 1F).

The cytotoxicity and properties of PEI-AuNCs. The toxicity of empty carrier PEI-AuNCs on PC-3 cells and human normal prostate epithelial cells RWPE-1 was examined using the CCK-8 assay. The results revealed that even after exposure to different concentrations for varying durations, the cell viability of both groups remained above 80%, and the growth and quantity of the cells were not significantly affected, indicating low cytotoxicity and excellent biocompatibility of the prepared PEI-AuNCs (Figure 2A). In addition, PC-3-GFP cells were employed as a cellular model. PEI-AuNCs@pGFP was co-cultured with the cells, and commercial transfection reagent Lip2000 served as a positive control (pGFP group) to evaluate the gene overexpression efficiency. As depicted in Figures 2B–2D, Lip2000 transfection resulted in 42% of cells displaying GFP-positive expression, but concurrently, there was a certain degree of reduction in cell count, indicating certain toxic side effects on the cells. In contrast, the GFP-positive efficiency of the PEI-AuNCs@pGFP group was 75%, with an overexpression efficiency significantly higher than the pGFP group ($p<0.01$), accompanied by a greater cell count. Furthermore, EMSA was conducted to analyze the protective ability of PEI-AuNCs for pDNA. The results suggested that, compared to free pCMTM5, PEI-AuNCs@pCMTM5 remained retained in the wells, unable to migrate within the electrophoresis field. In contrast, unprotected free pCMTM5 was completely degraded after cultivation with DNase-I (Figure 2E). The drug release results showed that free pCMTM5 exhibits rapid release in the medium, demonstrating a burst release effect, with approximately 60% released after 6 h and nearly complete release by 24 h. In contrast, the release of pCMTM5 encap-

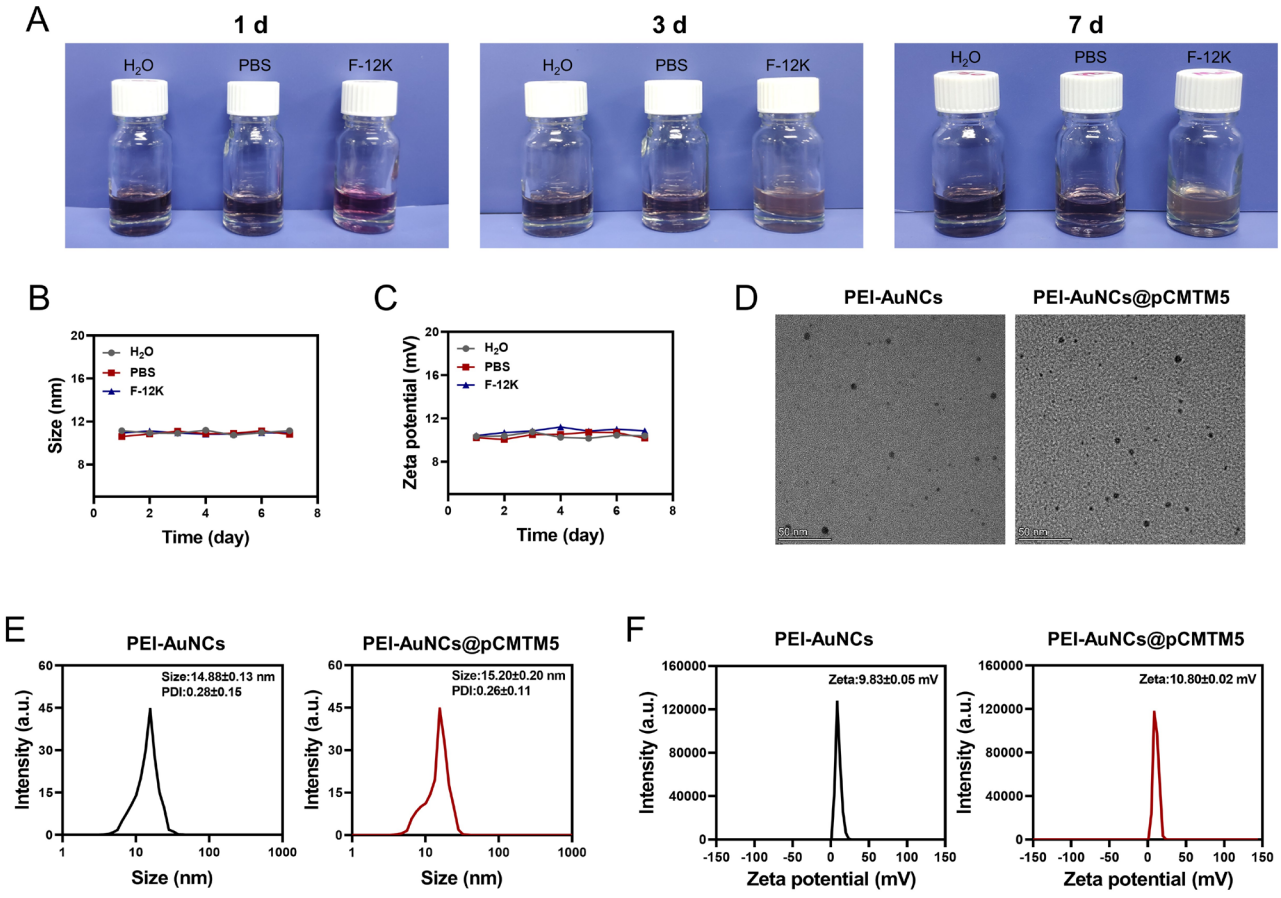

Figure 1. Characterization of PEI-AuNCs and PEI-AuNCs@pCMTM5. A) The dispersion status, B) the average particle size, and C) the zeta potential of PEI-AuNCs in water, PBS, and cell culture medium over seven days. D) The morphology of PEI-AuNCs and PEI-AuNCs@pCMTM5 were determined by transmission electron microscope (TEM). E) The average particle size and F) the zeta potential before and after the encapsulation of pCMTM5 were measured with dynamic light scattering (DLS). Three independent experiments were conducted in triplicate.

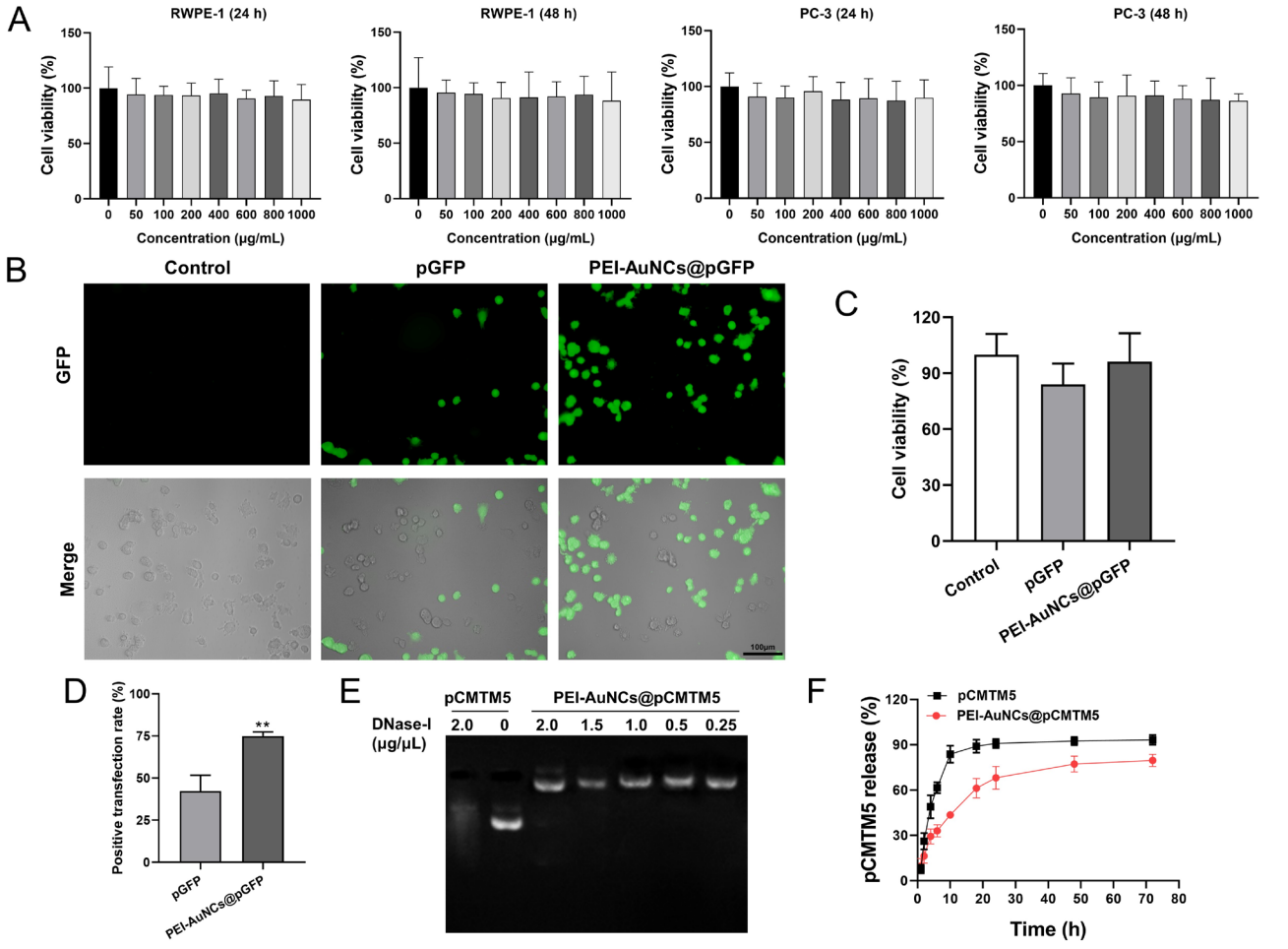

Figure 2. The cytotoxicity and properties of PEI-AuNCs. A) CCK-8 assay was employed to evaluate the toxicity of PEI-AuNCs on human normal prostate epithelial cells RWPE-1 and PC-3 cells at 24 and 48 h. B) Confocal laser scanning microscopy was utilized to observe the GFP overexpression efficiency in PC-3 cells. C) Cell viability following transfection was assessed via the CCK-8 assay. D) Quantitative representation of the positive transfection rate. E) Electrophoretic mobility shift assay (EMSA) was employed to demonstrate the protective effect of PEI-AuNCs on free DNA. Three independent experiments were conducted in triplicate. **p<0.01, compared with the pGFP group.

sulated in PEI-AuNCs@pCMTM5 is stable and sustained, indicating that PEI-AuNCs can protect the plasmid from enzymatic degradation while facilitating its transfection into cells and efficient release (Figure 2F).

The regulatory function of CMTM5 on EGFR expression and malignant cell progression. To elucidate the biological function of CMTM5 in the pathogenesis of PCa, CMTM5 overexpression was induced in PC-3 cells, and the transfection efficiency of CMTM5 was verified through qRT-PCR and western blot experiments. Compared to the PEI-AuNCs group, the transfection with PEI-AuNCs@pCMTM5 significantly elevated both CMTM5 mRNA and protein expression ($p<0.01$), and the transfection efficiency was superior to free pCMTM5 (Figures 3A, 3B). Further examination through qRT-PCR and western blot assessed the impact of CMTM5 overexpression on EGFR, the results showed no significant changes in EGFR expression at both the mRNA and protein expression levels among the groups, indicating that CMTM5 does not directly inhibit EGFR synthesis or promote EGFR degradation (Figures 3C, 3D). Moreover, the cell phenotypic experiments demonstrated the anti-cancer effect after transfection with PEI-AuNCs@pCMTM5 loaded with 2.5 μg pCMTM5. The proliferation capacity of PC-3 cells was significantly inhibited ($p<0.001$), and their migration and invasion capabilities were markedly reduced ($p<0.01$; $p<0.001$), with the effects being superior to those observed in the free pCMTM5 group (2.5 μg pCMTM5) (Figures 4A–4E). Additionally, under various treatments of RWPE-1 cells, as illustrated in Supplementary Figure S2, the outcomes revealed no significant variance in cell viability among the different groups, indicating the safety of PEI-AuNCs and the targeted anti-cancer efficacy of pCMTM5.

The mechanism of CMTM5 promoting EGFR endocytosis in PCa cells. To delve deeper into the regulatory mecha-

nism of CMTM5 on EGFR, cell surface EGFR expression was assessed through flow cytometry. The results revealed a significant reduction in cell surface EGFR expression in the PEI-AuNCs@pCMTM5 group compared to the PEI-AuNCs empty control ($p<0.01$, Figures 5A, 5B). Additionally, fluorescence microscopy was employed to detect the co-localization between EGFR and CMTM5. While the control group and the PEI-AuNCs group showed EGFR localization on the plasma membrane, transfection with PEI-AuNCs@pCMTM5 resulted in the internalization of the majority of EGFR into the cells, displaying a significant co-localization with CMTM5 (Figure 5C). Quantification of EGFR protein expression within the cells was further conducted through western blot experiments. The results demonstrated a significant decrease in cell surface EGFR expression ($p<0.01$) and a notable increase in intracellular EGFR protein expression ($p<0.01$) in the CMTM5-overexpressing PC-3 cells. Detection of total EGFR protein levels confirmed that the overexpression of CMTM5 had no significant impact on the total EGFR level (Figure 6A). Moreover, the results of immunoprecipitation confirmed that there was no mutual interaction between CMTM5 and EGFR, suggesting that CMTM5 does not directly interact with EGFR but regulates the malignant progression of PC-3 cells by promoting EGFR endocytosis (Figure 6B).

Discussion

Owing to the absence of clinical symptoms in the incipient stage of PCa, its definitive detection relies on prostate biopsies, alterations in PSA levels, a digital rectal examination (DRE) [29]. Research to date posits that cell surface proteins, glycoproteins, receptors, enzymes, and peptides serve as considered targets for PCa therapy [30]. Tumorigenesis emanates from aberrations in the normal expression of tumor suppressor genes or oncogenic factors [31, 32], and

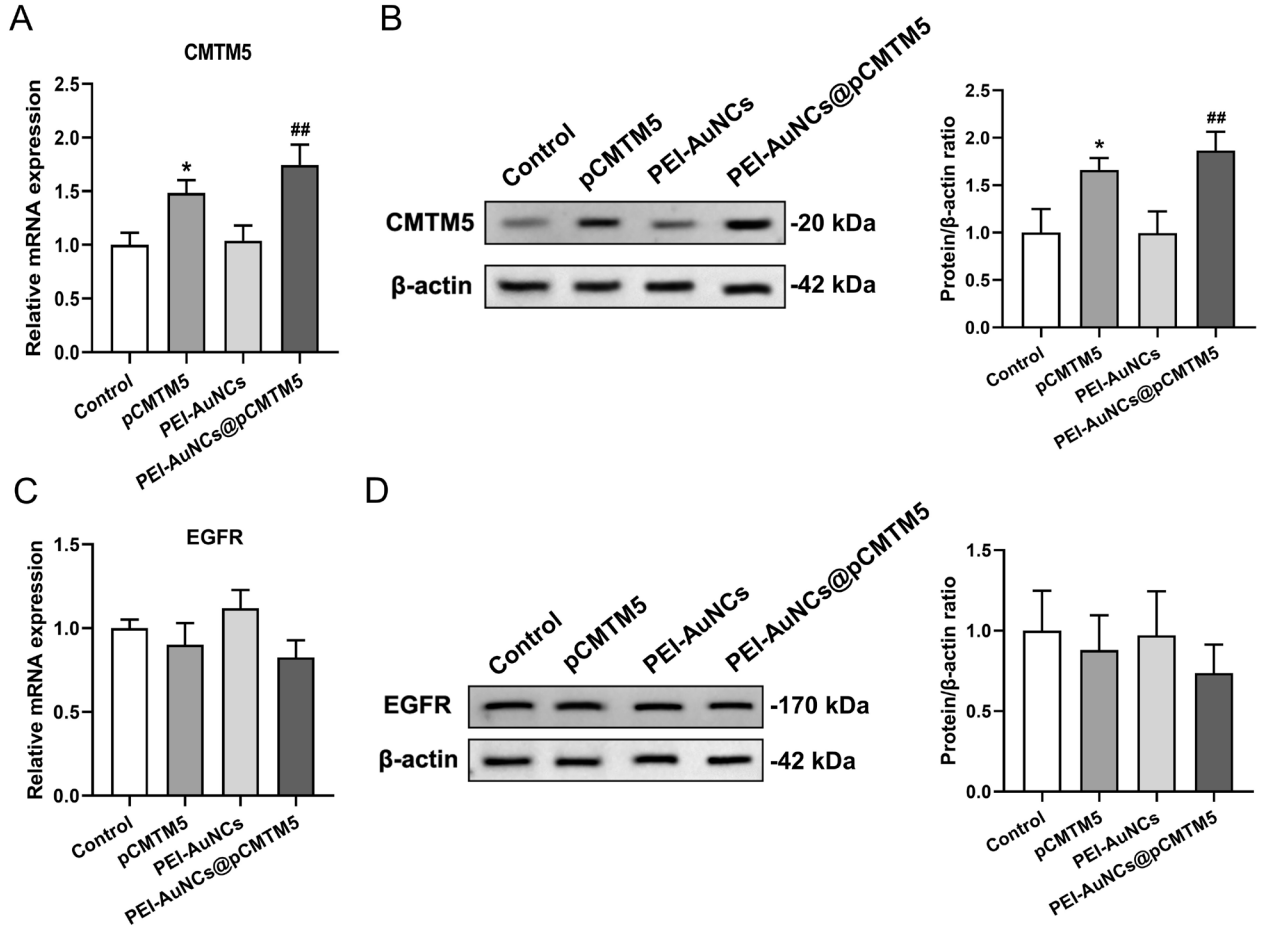

Figure 3. The efficiency of CMTM5 overexpression and its impact on EGFR expression. A) RT-qPCR was utilized to assess the mRNA levels of CMTM5. B) Western blot analysis was conducted to evaluate the protein expression of CMTM5. C) RT-qPCR was utilized to assess the mRNA levels of EGFR. D) Western blot analysis was conducted to evaluate the protein expression of EGFR. Three independent experiments were conducted in triplicate. *$p<0.05$, compared with the control group; ##$p<0.01$, compared with the PEI-AuNCs group.

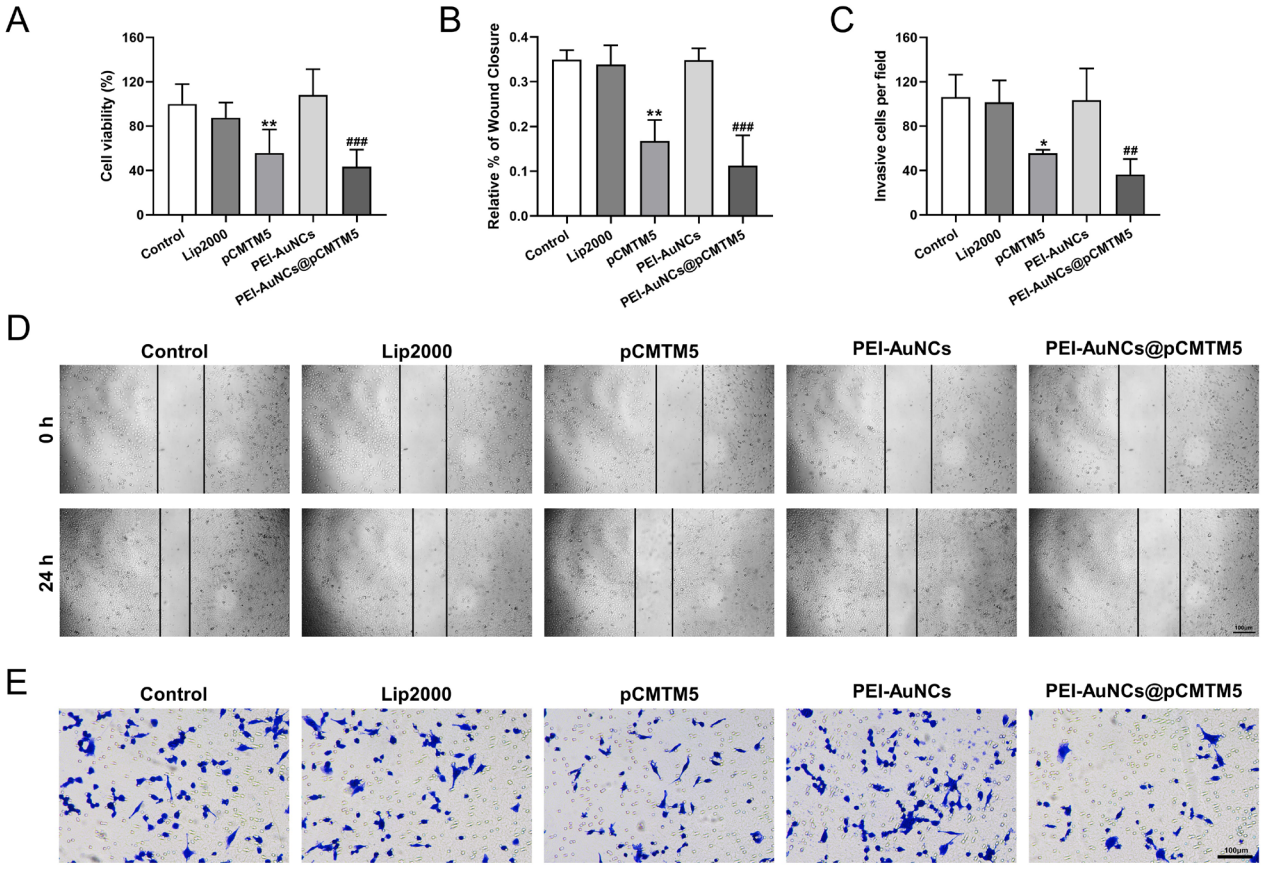

Figure 4. The impact of CMTM5 on the malignant progression of PCa cells. A) The CCK-8 assay was performed to assess the cell viability of PC-3 cells. B, D) The wound healing assay was employed to investigate alterations in the migratory capacity of PC-3 cells. C, E) The Transwell assay was utilized to detect variations in the invasive ability of PC-3 cells. Three independent experiments were conducted in triplicate. *p<0.05, **p<0.01, compared with the control group; ##p<0.01, ###p<0.001, compared with the PEI-AuNCs group.

comprehending the regulatory mechanisms in the cancer process can facilitate the discovery of novel anti-cancer modalities. Nucleic acids present a promising tool for therapeutic targets, wherein pDNA and small vector DNA are employed for repairing defective genes. Nevertheless, unlike small molecule therapy, nucleic acids necessitate delivery vehicles to shield them from nucleases and other environmental factors and to facilitate their entry into cells. Inorganic nanoparticles are emerging as promising carriers, presenting several advantages over conventional lipid carriers [33].

AuNCs serve as ideal delivery carriers, particularly for nucleic acid delivery applications, owing to a multitude of advantages, rendering them suitable for a wide range of biomedical applications [34]. A recent study has also underscored the efficient transfection of nucleic acids into mammalian cells mediated by gold nanoparticles, thereby being employed in the treatment of various types of cancers [35]. In this study, branched PEI was employed as a reducing and stabilizing agent in the synthesis of cationic AuNCs, and both the PEI-AuNCs and PEI-AuNCs@pCMTM5 underwent characterization through various physicochemical methods. The PEI-AuNCs were well dispersed, and the variations in particle size and zeta potential over time were minimal, indicating the commendable stability of the nanomaterials. Moreover, the morphology, average particle size, and zeta potential were assessed through TEM and DLS before and after the encapsulation of pCMTM5. The surface of PEI-AuNCs particles appeared rough, composed of numerous nanoscale pores and channels, which facilitates the encapsulation of biologically active molecules such as proteins, drugs, and genes within the nanoparticles, PEI-AuNCs@pCMTM5 also manifested uniformly dispersed spherical structures. Additionally, the measured average particle sizes of PEI-AuNCs and PEI-AuNCs@pCMTM5 adhered to the theoretical dimensions of nanoparticles capable of entering cells [36], and both stability and biocompatibility were satisfactory. Moreover, in comparison to the commercial transfection reagent Lip2000, the group treated with PEI-AuNCs carrying pGFP exhibited a higher positivity rate for GFP protein and a greater cell count, demonstrating

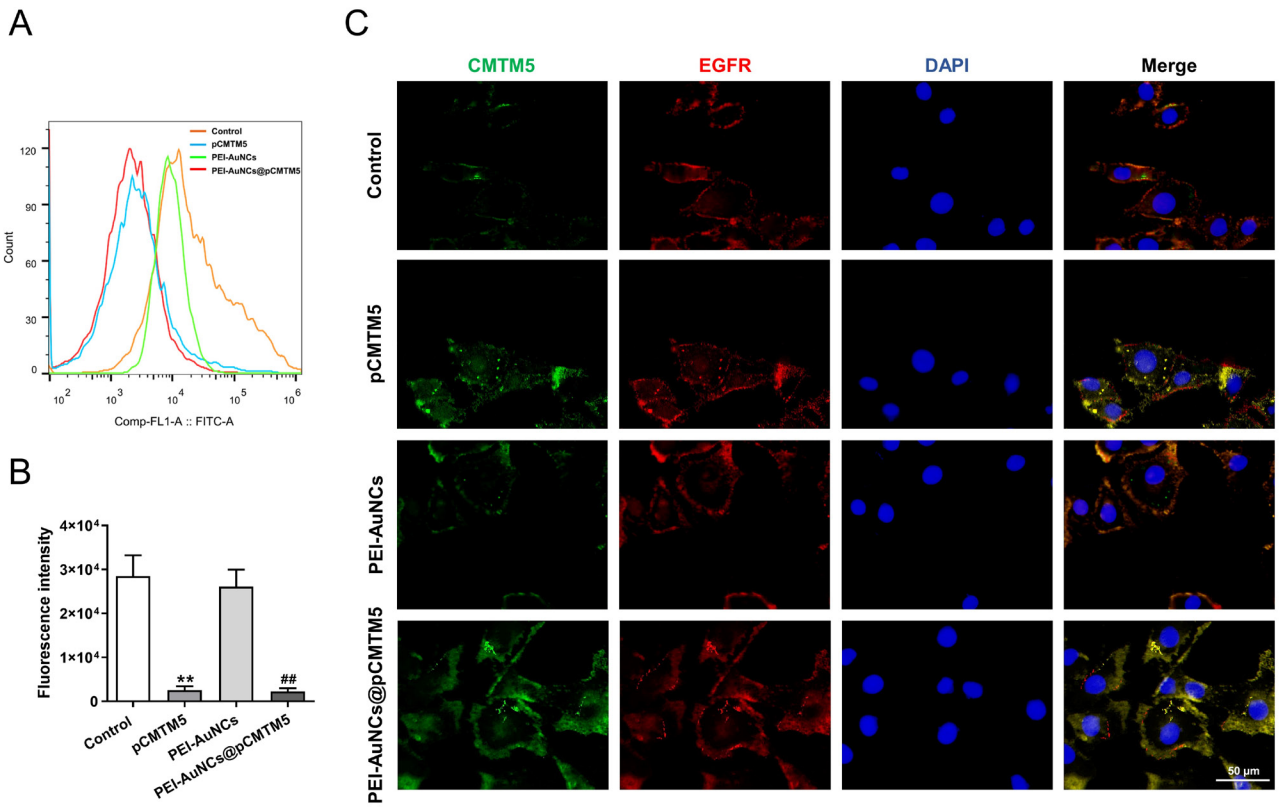

Figure 5. The influence of CMTM5 on EGFR internalization. A, B) Flow cytometry was employed to assess cell surface EGFR expression. C) Immunofluorescence was utilized to investigate the EGFR internalization and co-localization of CMTM5 and EGFR within the cells. Three independent experiments were conducted in triplicate. **p<0.01, compared with the control group; ##p<0.01, compared with the PEI-AuNCs group.

that PEI-AuNCs@pGFP not only possesses higher transfection efficiency but also exhibits lower toxic side effects. Furthermore, the structural integrity of the therapeutic gene is imperative to ensure its intended efficacy both *in vitro* and *in vivo*. An efficacious carrier should provide sufficient protection to pDNA against endonucleases degradation [37]. Thus, we evaluated this aspect via gel-based assays by combining a fixed concentration of PEI-AuNPs nanoconjugate with pCMTM5 DNA. DNase-I was employed as a model enzyme, effectuating DNA degradation by cleaving phosphodiester bonds [38]. Complexes were prepared as described in methods and subjected to varying concentrations of DNase I. The outcome of EMSA revealed that pCMTM5 DNA associated with positively charged PEI-AuNCs through electrostatic interactions, offering complete protection to the bound CMTM5 DNA. Furthermore, drug release results demonstrated that PEI-AuNCs can safeguard the efficient release of pCMTM5 in cells. Hence, PEI-AuNCs hold the potential to efficiently achieve targeted delivery of CMTM5 and represent a promising nanomaterial.

CMTM5, a multi-pass membrane protein consisting of 223 amino acids, has been documented for its potential anti-cancer properties [16]. We investigated the therapeutic impact of the CMTM5 gene in the delivery system targeting PCa, and the findings revealed that PEI-AuNCs stably delivered pCMTM5 DNA into PC-3 cells, markedly inhibiting the malignant progression of PCa, with superior efficacy compared to the administration of free pCMTM5. Nevertheless, the precise mechanism by which CMTM5 exerts its anti-PCa effects remains unclear. Presently, most research findings suggest that PCa cells exhibit malignant characteristics and metastasis in advanced stages, with the aberrant activation of the EGFR signaling pathway serving as a pivotal mechanism in PCa development [39]. Upon the upregulation of androgen receptor (AR) expression levels in non-androgen-dependent PCa cells, it was discovered that the AR could bind with EGFR, thereby inhibiting downstream PI3K pathway activation. However, with the employment of anti-androgen drugs, the interaction between AR and EGFR tended to decrease [40]. Based on the MARVEL domain and the multi-pass transmembrane domain contained within the structure of CMTM5, we speculate that CMTM5 is involved in the transport process of EGFR. In our study, following the overexpression of CMTM5, no significant alteration was

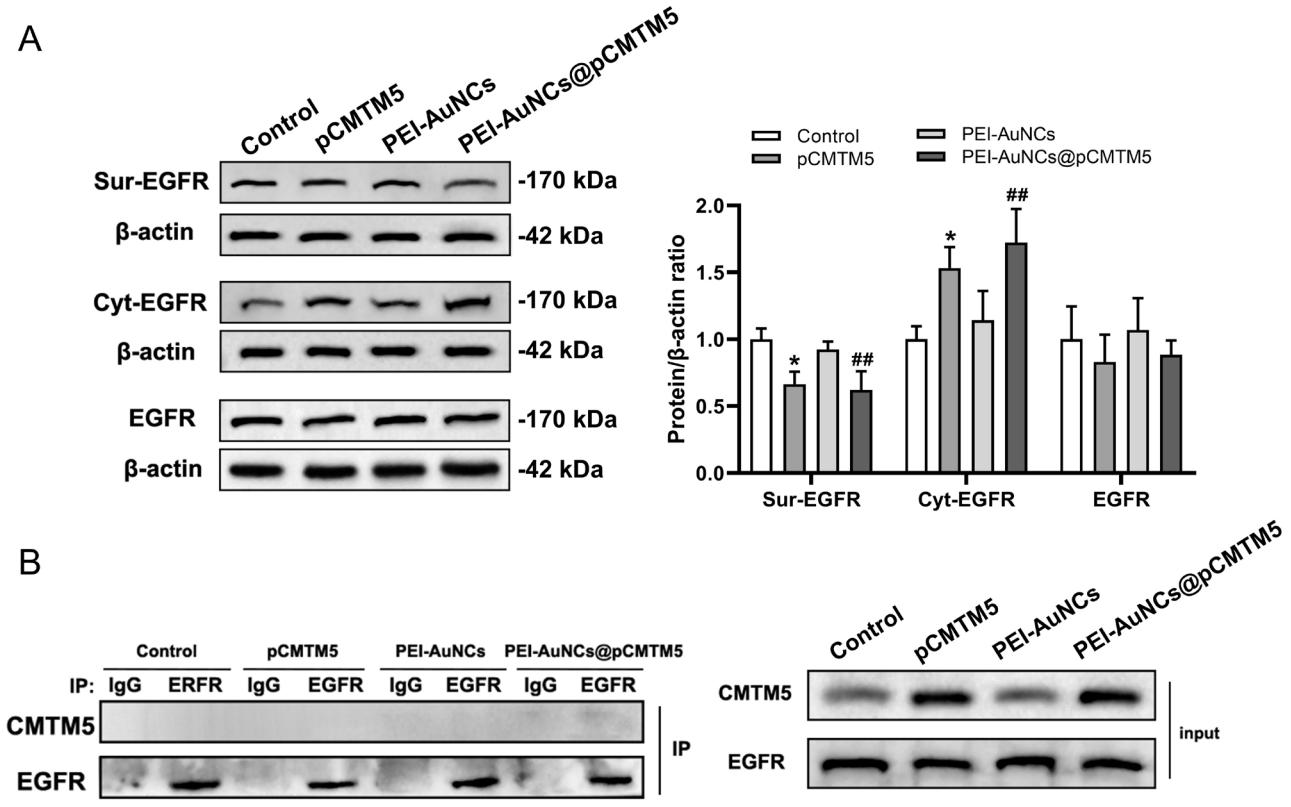

Figure 6. Detection of CMTM5 interaction with EGFR. A) Western blot analysis was conducted to assess the protein expression levels of total EGFR, as well as the protein expression levels of EGFR in the cell membrane and cytoplasm. B) Co-immunoprecipitation experiments were performed to investigate the interaction between CMTM5 and EGFR. Three independent experiments were conducted in triplicate. *p<0.05, compared with the control group; ##p<0.01, compared with the PEI-AuNCs group.

observed in the expression levels of EGFR mRNA and protein, indicating that CMTM5 does not facilitate the specific degradation of EGFR or inhibit the synthesis of EGFR.

Internalization and intracellular trafficking of the stimulated EGFRs play a crucial role in diversifying intracellular signals [41]. Previous studies have shown that CMTM8 is associated with the EGFR membrane complex, and could regulate EGFR signaling by accelerating membrane receptor internalization and subsequent degradation in tumor cells [42]. In addition, CMTM7 also inhibits cancer cell growth and represses oncogenic EGFR signaling by promoting EGFR internalization and further suppressing the Akt signaling pathway [43]. Yuan et al. [12] suggested that CMTM5 does not directly inhibit the synthesis of EGFR but speculated that it may suppress the progression of PCa by promoting the internalization and degradation of EGFR, thereby reducing the cell surface EGFR and weakening ligand-EGFR complex signaling. These findings prompted us to conduct further mechanistic studies to investigate whether CMTM5-overexpressing cells lead to an increase in the EGFR internalization rate. The outcomes of our experiments unveiled that the overexpression of CMTM5 in PC-3 cells expeditiously enhances the ligand-induced removal of EGFR from the cellular membrane surface, with the majority of EGFR being internalized into the cell and exhibiting a significant co-localization with CMTM5. The western blot results further elucidated that the overexpression of CMTM5 facilitates the internalization of EGFR, yet fails to elicit heightened specific degradation of EGFR, as evidenced by the constancy in total EGFR protein levels. Nevertheless, it is worth noting that CMTM5 and EGFR do not engage in direct reciprocal interactions. A large portion of the internalized receptors are destined for lysosomal degradation, thereby deactivating the signaling of the receptor [44]. As far as our knowledge extends, this is the first evidence confirming that CMTM5 guides EGFR into the endocytic pathway, facilitating the removal of EGFR from the cell membrane surface, thereby suppressing its oncogenic potential.

In summary, this study has employed the establishment of a well biocompatible PEI-AuNCs nano-delivery system to effectively deliver pCMTM5 to PCa cells. The experimental evidence validates CMTM5 as a novel negative regulatory factor in EGFR-induced signal transduction, exerting its anti-PCa effects by inducing EGFR endocytosis. With the

assistance of nanomaterial formulations, we posit that this combined approach is well-suited for *in vivo* targeted delivery of anti-cancer genes for therapeutic purposes. Further exploration of the *in vivo* mechanisms of biological distribution is warranted, and the current findings carry substantial significance for future in-depth investigations into the endocytosis and signal transduction mechanisms of EGFR.

Supplementary information is available in the online version of the paper.

Acknowledgments: This research was supported by the Wenzhou Science & Technology Bureau (Grant number: Y20210171).

References

[1] BRAY F, FERLAY J, SOERJOMATARAM I, SIEGEL RL, TORRE LA et al. Global cancer statistics 2018: GLOBOCAN estimates of incidence and mortality worldwide for 36 cancers in 185 countries. CA Cancer J Clin 2018; 68: 394–424. https://doi.org/10.3322/caac.21492

[2] JIA Y, ZHU LY, XIAN YX, SUN XQ, GAO JG et al. Detection rate of prostate cancer following biopsy among the northern Han Chinese population: a single-center retrospective study of 1022 cases. World J Surg Oncol 2017; 15: 165. https://doi.org/10.1186/s12957-017-1238-9

[3] ZHUO L, CHENG Y, PAN Y, ZONG J, SUN W et al. Prostate cancer with bone metastasis in Beijing: an observational study of prevalence, hospital visits and treatment costs using data from an administrative claims database. BMJ Open 2019; 9: e028214.

[4] CZERWIŃSKA M, BILEWICZ A, KRUSZEWSKI M, WEGIEREK-CIUK A, LANKOFF A. Targeted radionuclide therapy of prostate cancer—from basic research to clinical perspectives. Molecules 2020; 25: 1743. https://doi.org/10.3390/molecules25071743

[5] ASHRAFIZADEH M, HUSHMANDI K, RAHMANI MOGHADAM E, ZARRIN V, HOSSEINZADEH KASHANI S et al. Progress in Delivery of siRNA-Based Therapeutics Employing Nano-Vehicles for Treatment of Prostate Cancer. Bioengineering (Basel) 2020; 7: 91. https://doi.org/10.3 390/bioengineering7030091

[6] CATTRINI C, CASTRO E, LOZANO R, ZANARDI E, RUBAGOTTI A et al. Current treatment options for metastatic hormone-sensitive prostate cancer. Cancers (Basel) 2019; 11: 1355. https://doi.org/10.3390/cancers11091355

[7] BOETTCHER AN, USMAN A, MORGANS A, VANDERWEELE DJ, SOSMAN J et al. Past, current, and future of immunotherapies for prostate cancer. Front Oncol 2019; 9: 884. https://doi.org/10.3389/fonc.2019.00884

[8] LACOMBE L, HOVINGTON H, BRISSON H, MEHDI S, BEILLEVAIRE D et al. UGT2B28 accelerates prostate cancer progression through stabilization of the endocytic adaptor protein HIP1 regulating AR and EGFR pathways. Cancer Lett 2023; 553: 215994. https://doi.org/10.1016/j.canlet.2022.215994

[9] SAKANYAN V, IRADYAN N, ALVES DE SOUSA R. Targeted Strategies for Degradation of Key Transmembrane Proteins in Cancer. BioTech (Basel) 2023; 12: 57. https://doi.org/10.3390/biotech12030057

[10] ZHU JY, XIONG Y, ZHANG W, WAN J, WAN J. Endophilin B1 regulates EGFR endocytic degradation in prostate cancer cell. Cell Mol Biol (Noisy-le-grand) 2016; 62: 37–42.

[11] DAY KC, LORENZATTI HILES G, KOZMINSKY M, DAWSEY SJ, PAUL A et al. HER2 and EGFR Overexpression Support Metastatic Progression of Prostate Cancer to Bone. Cancer Res 2017; 77: 74–85. https://doi.org/10.1158/0008-5472.CAN-16-1656

[12] YUAN Y, SHENG Z, LIU Z, ZHANG X, XIAO Y et al. CMTM5-v1 inhibits cell proliferation and migration by downregulating oncogenic EGFR signaling in prostate cancer cells. J Cancer 2020; 11: 3762–3770. https://doi.org/10.7150/jca.42314

[13] XU G, DANG C. CMTM5 is downregulated and suppresses tumour growth in hepatocellular carcinoma through regulating PI3K-AKT signalling. Cancer Cell Int 2017; 17: 113. https://doi.org/10.1186/s12935-017-0485-8

[14] XU T, LI J, XIAO YB, LIU ZH, LI Q et al. [CMTM5 inhibits the tumor cell behavior of prostate cancer by downregulation of HER2]. Beijing Da Xue Xue Bao Yi Xue Ban 2010 ; 42: 386–390.

[15] XIAO YB, XIE J, ZHANG GX, LI J, HAO YC et al. [Inhibitory effect of CMTM5 on xenografted human prostatic cancer in nude mice]. Zhonghua Nan Ke Xue 2012; 18: 195–199.

[16] LI L, HU Y, CHEN D, ZHU J, BAO W et al. CMTM5 inhibits the development of prostate cancer via the EGFR/PI3K/AKT signaling pathway. Mol Med Rep 2022; 25: 17. https://doi.org/10.3892/mmr.2021.12533

[17] LI H, LI J, SU Y, FAN Y, GUO X et al. A novel 3p22.3 gene CMTM7 represses oncogenic EGFR signaling and inhibits cancer cell growth. Oncogene 2014; 33: 3109–3118. https://doi.org/10.1038/onc.2013.282

[18] JIN C, DING P, WANG Y, MA D. Regulation of EGF receptor signaling by the MARVEL domain-containing protein CKLFSF8. FEBS Lett 2005; 579: 6375–6382. https://doi.org/10.1016/j.febslet.2005.10.021

[19] WANG W, LI W, MA N, STEINHOFF G. Non-viral gene delivery methods. Curr Pharm Biotechnol 2013; 14: 46–60.

[20] HEIDARI R, ASSADOLLAHI V, KHOSRAVIAN P, MIRZAEI SA, ELAHIAN F. Engineered mesoporous silica nanoparticles, new insight nanoplatforms into effective cancer gene therapy. Int J Biol Macromol, 2023, 253: 127060. https://doi.org/10.1016/j.ijbiomac.2023.127060

[21] SHARMA S, DAS S, KAUSHIK K, YADAV A, PATRA A et al. Unveiling the Long-Lived Emission of Copper Nanoclusters Embedded in a Protein Scaffold. J Phys Chem Lett 2023; 14: 8979–8987. https://doi.org/10.1021/acs.jpclett.3c01877

[22] ALONSO MC, TRAPIELLA-ALFONSO L, FERNÁNDEZ JMC, PEREIRO R, SANZ-MEDEL A. Functionalized gold nanoclusters as fluorescent labels for immunoassays: application to human serum immunoglobulin E determination. Biosens Bioelectron 2016; 77: 1055–1061. https://doi.org/10.1016/j.bios.2015.08.011

[23] YUAN Q, WANG Y, ZHAO L, LIU R, GAO F et al. Peptide protected gold clusters: chemical synthesis and biomedical applications. Nanoscale 2016; 8: 12095–12104. https://doi.org/10.1039/c6nr02750d

[24] LEI Y, TANG L, XIE Y, XIANYU Y, ZHANG L et al. Gold nanoclusters-assisted delivery of NGF siRNA for effective treatment of pancreatic cancer. Nat Commun 2017; 8: 15130. https://doi.org/10.1038/ncomms15130

[25] PORRET E, LE GUÉVEL X, COLL JL. Gold nanoclusters for biomedical applications: toward in vivo studies. J Mater Chem B 2020; 8: 2216–2232. https://doi.org/10.1039/c9tb02767j

[26] ZHANG J, LEI W, MENG Y, ZHOU C, ZHANG B et al. Expression of PEI-coated gold nanoparticles carrying exogenous gene in periwinkle mesophyll cells and its practice in huanglongbing research. iScience 2022; 25: 104479. https://doi.org/10.1016/j.isci.2022.104479

[27] DEHSHAHRI A, ALHASHEMI SH, JAMSHIDZADEH A, SABAHI Z, SAMANI SM et al. Comparison of the effectiveness of polyethylenimine, polyamidoamine and chitosan in transferring plasmid encoding interleukin-12 gene into hepatocytes. Macromol Res 2013; 21: 1322–1330. https://doi.org/10.1007/s13233-013-1180-9

[28] LI M, GUO Z, YANG H, LIU Y, TONG Y et al. Electrochemical sensor based on polyethyleneimine-aunps-anthraquinone-2-carboxylic acid nanocomposite for cysteine detection. Int J Electrochem Sci 2019; 14: 943–956. https://doi.org/10.20964/2019.01.72

[29] EGIDI MG, COCHETTI G, GUELFI G, ZAMPINI D, DIVERIO S et al. Stability assessment of candidate reference genes in urine sediment of prostate cancer patients for miRNA applications. Dis Markers 2015; 2015: 973597. https://doi.org/10.1155/2015/973597

[30] DIAO W, CAI H, CHEN L, JIN X, LIAO X et al. Recent advances in prostate-specific membrane antigen-based radiopharmaceuticals. Curr Top Med Chem 2019; 19: 33–56. https://doi.org/10.2174/1568026619666190201100739

[31] MOHAN CD, RANGAPPA S, PREETHAM HD, NAYAKA SC, GUPTA VK et al. Targeting STAT3 signaling pathway in cancer by agents derived from Mother Nature. Semin Cancer Biol 2022: 80: 157–182. https://doi.org/10.1016/j.semcancer.2020.03.016

[32] KASHYAP D, TULI HS, YERER MB, SHARMA A, SAK K et al. Natural product-based nanoformulations for cancer therapy: Opportunities and challenges. Semin Cancer Biol 2021; 69: 5–23. https://doi.org/10.1016/j.semcancer.2019.08.014

[33] LIN G, REVIA RA, ZHANG M. Inorganic Nanomaterial-Mediated Gene Therapy in Combination with Other Antitumor Treatment Modalities. Adv Funct Mater 2021; 31: 2007096. https://doi.org/10.1002/adfm.202007096

[34] KOTCHERLAKOTA R, SRINIVASAN DJ, MUKHERJEE S, HAROON MM, DAR GH et al. Engineered fusion protein-loaded gold nanocarriers for targeted co-delivery of doxorubicin and erbB2-siRNA in human epidermal growth factor receptor-2+ ovarian cancer. J Mater Chem B 2017; 5: 7082–7098. https://doi.org/10.1039/c7tb01587a

[35] HOSSEINI SA, KARDANI A, YAGHOOBI H. A comprehensive review of cancer therapies mediated by conjugated gold nanoparticles with nucleic acid. Int J Biol Macromol 2023; 253: 127184. https://doi.org/10.1016/j.ijbiomac.2023.127184

[36] GRACZYK A, PAWLOWSKA R, JEDRZEJCZYK D, CHWOROS A. Gold nanoparticles in conjunction with nucleic acids as a modern molecular system for cellular delivery. Molecules 2020; 25: 204. https://doi.org/10.3390/molecules25010204

[37] LAYEK B, HALDAR MK, SHARMA G, LIPP L, MALLIK S et al. Mol Pharm 2014; 11: 982–994. https://doi.org/10.1021/mp400633r

[38] KOTCHERLAKOTA R, VYDIAM K, JEYALAKSHMI SRINIVASAN D, MUKHERJEE S, ROY A et al. Restoration of p53 Function in Ovarian Cancer Mediated by Gold Nanoparticle-Based EGFR Targeted Gene Delivery System. ACS Biomater Sci Eng 2019; 5: 3631–3644. https://doi.org/10.1021/acsbiomaterials.9b00006

[39] OTA H, SATO H, MIZUMOTO S, WAKAI K, YONEDA K et al. Switching mechanism from AR to EGFR signaling via 3-O-sulfated heparan sulfate in castration-resistant prostate cancer. Sci Rep 2023; 13: 11618. https://doi.org/10.1038/s41598-023-38746-x

[40] PERNER S, CRONAUER MV, SCHRADER AJ, KLOCKER H, CULIG Z et al. Adaptive responses of androgen receptor signaling in castration-resistant prostate cancer. Oncotarget 2015; 6: 35542–35555. https://doi.org/10.18632/oncotarget.4689

[41] WEE P, WANG Z. Epidermal Growth Factor Receptor Cell Proliferation Signaling Pathways. Cancers (Basel) 2017; 9: 52. https://doi.org/10.3390/cancers9050052

[42] JIN C, DING P, WANG Y, MA D. Regulation of EGF receptor signaling by the MARVEL domain-containing protein CKLFSF8. FEBS Lett 2005; 579: 6375–6382. https://doi.org/10.1016/j.febslet.2005.10.021

[43] LI H, LI J, SU Y, FAN Y, GUO X et al. A novel 3p22. 3 gene CMTM7 represses oncogenic EGFR signaling and inhibits cancer cell growth. Oncogene 2014; 33: 3109–3118. https://doi.org/10.1038/onc.2013.282

[44] MODICA TME, DITURI F, MANCARELLA S, PISANO C, FABREGAT I et al. Calcium Regulates HCC Proliferation as well as EGFR Recycling/Degradation and Could Be a New Therapeutic Target in HCC. Cancers (Basel) 2019; 11: 1588. https://doi.org/10.3390/cancers11101588

https://doi.org/10.4149/neo_2024_231018N544

The role of polyethylenimine-functionalized gold nanoclusters carrying plasmid CMTM5 in impeding the malignant progression of prostate cancer cells by promoting EGFR endocytosis

Linjin LI[1,#], Chengpeng LI[1,#], Feilong MIAO[1], Wu CHEN[1], Xianghui KONG[1], Ruxian YE1, Rui FENG[2,*]

Supplementary Information

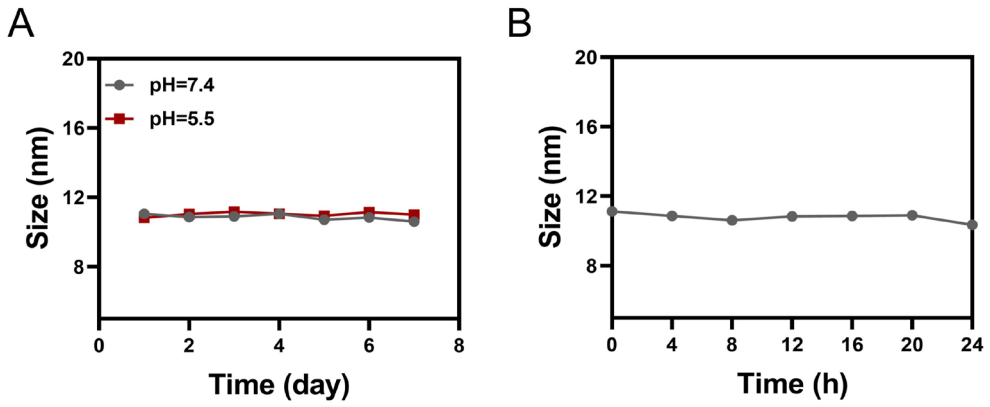

Supplementary Figure S1. A) The average particle size of PEI-AuNCs was examined under different pH conditions (neutral and acidic) over seven days, and B) continuously measured at six time points within the initial 24 h

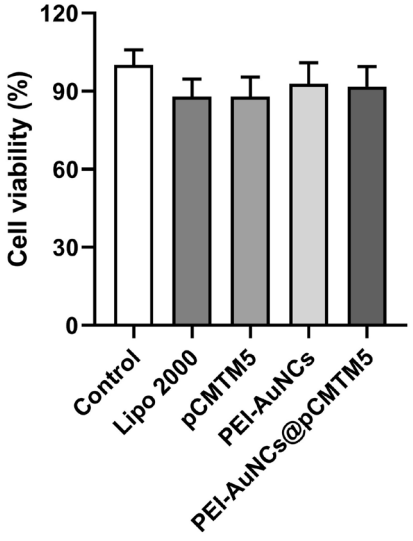

Supplementary Figure S2. The CCK-8 assay was performed to assess the cell viability of RWPE-1 cells.